

Self-consistent theory of 2×2 pair density waves in kagome superconductors

Meng Yao,¹ Yan Wang,¹ Da Wang,^{1,2,*} Jia-Xin Yin,^{3,†} and Qiang-Hua Wang^{1,2,‡}

¹*National Laboratory of Solid State Microstructures & School of Physics, Nanjing University, Nanjing 210093, China*

²*Collaborative Innovation Center of Advanced Microstructures, Nanjing University, Nanjing 210093, China*

³*Department of Physics, Southern University of Science and Technology, Shenzhen, Guangdong 518005, China*

Pair density wave (PDW) is an intriguing quantum matter proposed in the frontier of condensed matter physics. However, the existence of PDW in microscopic models has been rare. In this work, we obtain, by Ginzburg-Landau arguments and self-consistent mean field theory, novel $2a_0 \times 2a_0$ PDW on the kagome lattice arising from attractive on-bond pairing interactions and the distinct Bloch wave functions near the p-type van Hove singularity. The PDW state carrying three independent wave-vectors, the so-called 3Q PDW, is nodeless and falls into two topological classes characterized by the Chern number $C = 0$ or $C = \pm 2$. The chiral ($C = \pm 2$) PDW state presents a rare case of interaction driven topological quantum state without the requirement of spin-orbit coupling. Finally, we analyze the stabilities and properties of these PDWs intertwining with charge orders, and discuss the relevance of our minimal model to recent experimental observations in kagome superconductors. Our theory not only elucidates the driving force of the chiral PDW, but also predicts strongly anisotropic superconducting gap structure in the momentum space and quantized transverse thermal conductivity that can be tested in future experiments.

I. INTRODUCTION

Pair density wave (PDW) is an exotic superconducting (SC) order with spatially nonuniform order parameters caused by condensing the Cooper pairs with nonzero center of mass momenta. It was first conceived to exist in superconductors with a strong spin-exchange field such that two paired equal-energy electrons do not have opposite momenta anymore [1, 2]. Such a SC state is called FFLO state and has possibly been realized in cold atom systems [3–5]. On the other hand, in cuprates without time-reversal symmetry breaking, the PDW with nonzero pairing momentum has also been proposed phenomenologically to serve as a mother state to generate various daughter states, dubbed as intertwined orders, in the pseudogap phase [6–8]. Such a proposal subsequently triggered extensive studies of PDW in recent years [7, 8], and some signatures of the PDW states have been reported in a series of materials such as cuprate and iron-based superconductors [9–22], heavy fermion material UTe₂ [23, 24], kagome compound AV₃Sb₅ [25], and other materials [26, 27]. Although many theoretical successes have been achieved at the phenomenological level [28–35], the existence of spontaneous PDW is rare in microscopic models, since the usual Cooper pairing with zero momentum always enjoys perfect Fermi surface (FS) nesting in the particle-particle channel and thus leaves no room for PDW, unless the interactions are strong enough to break this weak-coupling picture of Cooper instability. Extensive efforts have been made [36–68], but the existence of long-range PDW order has not been conclusively demonstrated in realistic models.

In this work, we show that the PDW is favored by on-bond pairing interactions on the kagome lattice near the upper p-type van Hove (vH) filling. The resulting $2a_0 \times 2a_0$ PDW ground states and Bogoliubov-de Gennes (BdG) quasiparticles are analyzed within the Ginzburg-Landau (GL) and self-consistent mean field calculations. Interestingly, such PDW states are found to intertwine with the charge density wave (CDW) orders and are likely to exist in the kagome superconductors AV₃Sb₅, which are intensively studied in the past few years [69–76].

II. PDW INSTABILITY NEAR UPPER VH FILLING

We study the kagome lattice as shown in Fig. 1(a), with the three sublattices labeled by A, B, and C, respectively. From the tight-binding Hamiltonian

$$H_0 = -t \sum_{(ij)\sigma} (c_{i\sigma}^\dagger c_{j\sigma} + \text{H.c.}), \quad (1)$$

with only the nearest neighbor hopping t (taken as energy unit), the band structure is shown in Fig. 1(b). There are two vH fillings $(4 \pm 1)/12$, as indicated by the two dashed lines corresponding to chemical potential $\mu = 0$ and -2 , respectively. For these fillings, their FSs are exactly the same but their Bloch wave functions are quite different. For the upper vH filling as shown in Fig. 1(c), the wave function at each M -point is contributed by purely one sublattice, hence, called p-type. Instead, for the lower vH filling as shown in Fig. 1(d), the wave function at each M is contributed by mixing two sublattices, hence called m-type. The difference between these two vH fillings leads to distinct properties as discussed in previous studies [61, 77–83]. Here, we show that the particular p-type vH singularity can lead to PDW instability instead of the usual SC. If the onsite pairing interaction is

* dawang@nju.edu.cn

† yinjax@sustech.edu.cn

‡ qhwang@nju.edu.cn

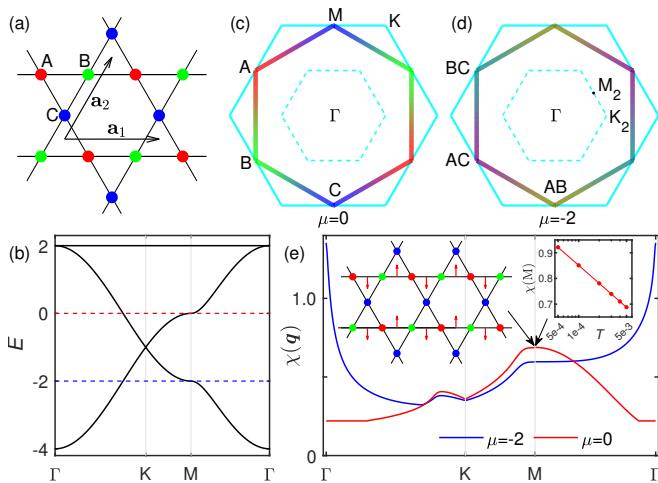


FIG. 1. (a) Kagome lattice structure with the three sublattices labeled by A (red), B (green) and C (blue), respectively. \mathbf{a}_1 and \mathbf{a}_2 denote two primitive translation vectors with length a_0 . (b) Band dispersion along Γ -K-M- Γ , with the red and blue dashed lines indicating two vH fillings. The FS at the upper vH filling is plotted in (c) in the first Brillouin zone (BZ) with color-scaled sublattice weight. The folded BZ for the $2a_0 \times 2a_0$ unitcell is given by dashed lines. (d) is similar to (c) but for the lower vH filling. (e) The largest spin-singlet pairing susceptibility $\chi(\mathbf{q})$ for upper (red) and lower (blue) vH fillings at temperature $T = 0.005$. For one M -point at the upper vH filling, the left inset illustrates the eigen mode with arrow directions (lengths) representing the pairing phases (amplitudes) for relevant bonds (up to a global phase), and the right inset shows the logarithmic temperature dependence of $\chi(M)$.

suppressed by *e.g.* Hubbard repulsion, the leading pairing interaction is expected to be on the nearest neighbor bond. For this reason, by choosing the basis of on-bond fermion pairs $b_{iI} = c_{i+\delta, \sigma} c_{i+\delta', \sigma'}$ (indices other than unitcell position i are grouped into I), we calculate the zero-frequency pairing susceptibility $\hat{\chi}(\mathbf{q})$ with the matrix element $\chi_{IJ}(\mathbf{q}) = \frac{1}{L^d} \sum_{ij} \int_0^\beta d\tau \langle b_{iI}(\tau) b_{jJ}^\dagger(0) \rangle e^{i\mathbf{q} \cdot (\mathbf{r}_j - \mathbf{r}_i)}$. For each \mathbf{q} , we diagonalize $\hat{\chi}(\mathbf{q})$ to obtain its eigenvalues and eigenvectors. The leading eigenvalue $\chi(\mathbf{q})$ in spin-singlet channel at the upper vH filling is plotted in Fig. 1(e). One can see that the highest peak occurs at M , which diverges logarithmically with decreasing temperature (see right inset), indicating the PDW instability with $2a_0 \times 2a_0$ period. Such an instability can be understood by the fact that on-bond pairings only combine different sublattices, hence, different M -points for the p-type vH filling, leading to a finite momentum $\mathbf{M}_3 = \mathbf{M}_1 + \mathbf{M}_2$ (mod reciprocal vectors) of the Cooper pair. The corresponding eigenvector at one M is illustrated in the left inset of Fig. 1(e). The arrows indicate the pairing phases (up to a global one) on the relevant bonds. The eigen modes at the other two M -points can be obtained by C_3 rotations. As a comparison, we also plot the susceptibility at the lower vH filling in Fig. 1(e), where the divergence occurs at Γ , indicating the usual SC ground

state.

III. PDW GROUND STATES AND BDG QUASIPARTICLES

The above analysis indicates three degenerate PDW modes at different M -points, which can be associated with three order parameters $\psi_{1,2,3}$, respectively. Their interplay will lead to different PDW ground states. In terms of $\psi_{1,2,3}$, we construct a three-component GL free energy up to the fourth order by requiring the following symmetries: C_3 -rotation, momentum conservation, time reversal (TR) and U(1) gauge symmetries. Under these constraints, the second order term can only be $|\psi_i|^2$, and the fourth order terms can be $|\psi_i|^4$, $|\psi_i|^2|\psi_j|^2$ and $(\psi_i^{*2}\psi_j^2 + \text{c.c.})$. Therefore, we write the uniform GL free energy as

$$F_{\text{PDW}} = -\alpha \sum_i |\psi_i|^2 + \beta_1 \sum_i |\psi_i|^4 + \beta_2 \sum_{i < j} |\psi_i|^2 |\psi_j|^2 + \beta_3 \sum_{i < j} (\psi_i^{*2} \psi_j^2 + \text{c.c.}), \quad (2)$$

where α and $\beta_{1,2,3}$ are real numbers. Clearly, a large positive β_2 favors nematicity (with unequal $|\psi_i|$), while a positive β_3 causes phase frustration and favors TR breaking. By varying β_2 and β_3 under a fixed value of β_1 , we obtain four possible phases, as shown in Fig. 2(a). Following the usual convention, we use the number of nonzero components to label different PDW phases. In the 1Q phase, only one component is nonzero, which is an extremely nematic PDW. In the 2Q phase, the two nonzero components are found to have the same amplitude but with a relative phase $\pi/2$, which is a chiral 2Q PDW state. The 3Q phases with $|\psi_1| = |\psi_2| = |\psi_3|$ are further divided into two classes: real (up to a global phase) and chiral (with relative phase $2\pi/3$ or $\pi/3$ between each two components). These two types of PDWs can also be denoted as s - and $d \pm id$ wave, respectively, in view of the phase winding along the holo hexagons and the small triangles (detached from the holo hexagons).

Next, let us examine the BdG quasiparticles in these PDW states. A common belief is that the Fermi surface cannot be fully gapped since the pairing electrons with momenta \mathbf{k} and $-\mathbf{k} + \mathbf{Q}$ cannot reside on the FS simultaneously for all momenta [8]. Here, however, we show that this belief is not true for the 3Q PDW states. In Fig. 2(b), we plot the quasiparticle bands in the folded BZ for the chiral 3Q PDW state (the real 3Q state is similar and not shown). The 3Q-PDW opens a full excitation gap, with the gap minimum Δ_m near M_2 . This full gap behavior is not a numerical artifact but intrinsic to the 3Q PDW states, which is fundamentally different from the 1Q and 2Q states with residual FSs (see Fig. S1 in Supplementary Material). The full gap in the 3Q PDW states can be understood by a higher order pair scattering process as illustrated in Fig. 2(c): $\mathbf{k} \rightarrow -\mathbf{k} + \mathbf{Q}_1 \rightarrow \mathbf{k} + \mathbf{Q}_1 + \mathbf{Q}_2 \rightarrow -\mathbf{k} + \mathbf{Q}_1 + \mathbf{Q}_2 + \mathbf{Q}_3$.

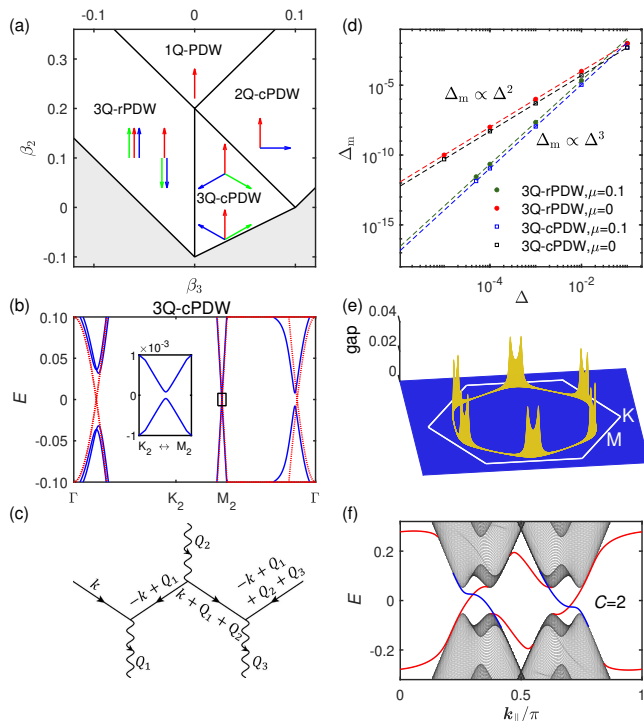


FIG. 2. (a) PDW phase diagram of the GL theory for $\beta_1 = 0.1$. The three colored arrows denote (ψ_1, ψ_2, ψ_3) on the complex plane, up to C_3 -rotations and a global phase. In each 3Q phase, two degenerate patterns are given. The shaded region indicates the absence of a free energy minimum up to fourth order. For these PDW names, “r” means real and “c” means chiral. (b) The low-energy BdG quasiparticle bands in the folded BZ for the chiral 3Q states for $\Delta = |\psi_i| = 0.02$ and $\mu = 0.1$, with the zoom-in near M_2 shown as the inset. For comparison, the normal state bands are given as red dashed lines. (c) Example of the 3rd-order pair scattering diagrams. The solid line denotes fermion and dashed line denotes pairing field ψ (ψ^*) incoming (outgoing) with respect to the three-point vertices. Note that $\mathbf{Q}_{1,2,3} = -\mathbf{Q}_{1,2,3}$ and $\mathbf{Q}_1 + \mathbf{Q}_2 + \mathbf{Q}_3 = 0$ up to reciprocal vectors. (d) The gap minimum Δ_m in the real and chiral 3Q PDW states versus Δ at ($\mu = 0$) or away from ($\mu = 0.1$) the vH filling. (e) The quasiparticle gap near the normal state FS for the chiral 3Q PDW state in (b). (f) The low-energy bands for the chiral 3Q PDW state for $\Delta = 0.4$ on a cylinder with open boundaries along the \mathbf{a}_1 direction, showing two edge states on each boundary (red or blue), consistent with the total Chern number $C = 2$.

Since $\mathbf{Q}_1 + \mathbf{Q}_2 + \mathbf{Q}_3 = 0$ (up to reciprocal vectors), the third order process always connects $(\mathbf{k}, -\mathbf{k})$ for any \mathbf{k} and thus gaps out the entire FS. In this mechanism, the minimal gap is expected to be proportional to the cube of the order parameter amplitude $\Delta = |\psi_i|$, which is in good agreement with the numerical results at $\mu = 0.1$ as shown in Fig. 2(d). Note that if the system is exactly at the upper vH filling ($\mu = 0$), the second order process is enough to connect $(\mathbf{k}, \mathbf{k} + \mathbf{Q})$ of equal energy due to the perfect FS nesting. Therefore, the power exponent is reduced from 3 to 2 as seen in Fig. 2(d). For comparison with experiments, we plot the excitation gap

near the normal state FS in the unfolded BZ as shown in Fig. 2(e), by calculating the quasiparticle spectral function thereon (see Fig. S2 in Supplementary Material). The \mathbf{k} -dependent excitation gap is maximal (minimal) in the $\Gamma - M$ ($\Gamma - K$) direction. This seems to be consistent with the gap variation on one out of several FSs (in the absence of CDW gap) in a recent ARPES experiment [84] in AV_3Sb_5 up to the resolution uncertainties. In the fully gapped 3Q PDW states, the Chern number C is well defined, which is found to be 0 for the real PDW and ± 2 for the chiral ones. In Fig. 2(f), we show the edge states (two chiral edge modes on each boundary) for the chiral 3Q phase on a cylinder with open boundaries along the \mathbf{a}_1 direction. (Here, a large PDW pairing is assumed to reduce the finite size effect but without loss of the qualitative physics.) It is remarkable that such a topological chiral PDW could emerge from an interacting model without the necessity of spin-orbit coupling. Moreover, the chiral edge states are Weyl fermions, and should exhibit a quantized thermal Hall conductance, $\kappa_{xy}/T = C(\pi^2/3)(k_B^2/h)$ [85], which could be probed in future experiments.

IV. SELF-CONSISTENT MEAN FIELD CALCULATIONS

The above GL analysis indicates four PDW candidate ground states depending on the phenomenological GL parameters $\beta_{1,2,3}$. In this section, we narrow down and sharpen the results by self-consistent mean field calculations. We consider on-bond pairing interaction

$$-J \sum_{\langle ij \rangle \sigma \tau} (\sigma c_{i\sigma}^\dagger c_{j\bar{\sigma}}^\dagger) (\tau c_{j\bar{\tau}} c_{i\tau}), \quad (3)$$

where $\langle ij \rangle$ denote the nearest neighbor bonds, $\bar{\sigma} = -\sigma = \pm 1$ and $\bar{\tau} = -\tau = \pm 1$. We require self-consistency in the order parameter $\Delta_{ij} = \sum_{\tau} \tau \langle c_{j\bar{\tau}} c_{i\tau} \rangle$. Since the PDW instability occurs at M , we impose the $2a_0 \times 2a_0$ periodicity on the lattice. After self-consistency is achieved, we also calculate the onsite and on-bond charge densities $n_i = \langle c_{i\sigma}^\dagger c_{i\sigma} \rangle$ and $\chi_{ij} = \langle c_{j\sigma}^\dagger c_{i\sigma} \rangle$, from the latter we obtain the current $\text{Im}(\chi_{ij})$ and valence-bond strength $\text{Re}(\chi_{ij})$.

Our results are summarized in the phase diagram Fig. 3(a). Near the lower vH filling, we find the usual SC with the pairing pattern shown in Fig. 3(b). While near the upper vH filling, we obtain 3Q PDW states only. Larger supercells have been used to check the robustness of these $2a_0 \times 2a_0$ PDW. In the real 3Q PDW phase as shown in Fig. 3(c), one can see that the PDW induces secondary onsite and valence-bond CDWs. The chiral 3Q states are more complicated. It further induces different types of loop current (LC) orders, according to which we further divide it into four subphases as shown in Figs. 3(d-g). For both the real and chiral 3Q PDWs, secondary CDW orders are induced, manifesting intertwining between these two types of orders. The strong intertwining between PDW and other orders has been

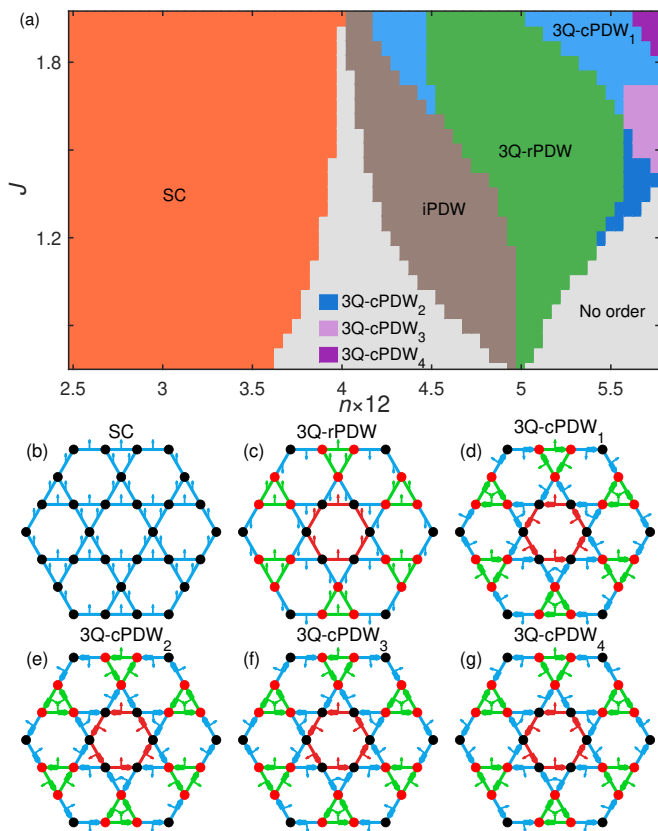


FIG. 3. (a) Mean field phase diagram with respect to on-bond pairing interaction J and filling level n at $T = 0.005$, with different phases represented by different colors. The brown region denotes incommensurate PDW (iPDW). The pairing patterns of different phases are illustrated in (b) to (g) as arrows starting from each bond center. In addition, the induced CDW patterns are also given, with black/red dots denoting n_i , blue/red/green bonds denoting $\text{Re}\chi_{ij}$, and arrows along each bond denoting $\text{Im}\chi_{ij}$.

proposed to explain the variety of competing orders in the pseudogap phase of cuprates [7]. Our study here is clear evidence of the intertwining between PDW and CDW on the kagome lattice based on microscopic calculations. On the other hand, in the brown region below the upper vH filling, we find larger unitcells may further lower the total energy. This is consistent with the fact that the momentum with the largest $\chi(\mathbf{q})$ varies gradually from M to K (not shown) as the filling level decreases from $\frac{5}{12}$ (upper vH) to $\frac{1}{4}$ (Dirac point). Therefore, we attribute this region as incommensurate PDW.

V. PDW ON CDW: POSSIBILITY IN AV_3Sb_5

Finally, we examine the possibilities of these PDWs in AV_3Sb_5 , for which the superconductivity occurs inside the CDW state [69–76]. We have seen that the PDWs can induce CDWs. Conversely, the background of CDWs will inevitably affect the PDWs. In AV_3Sb_5 , the microscopic

mechanism of (chiral) CDW is still an unsettled issue. For our purpose, in order to obtain robust LC orders, we adopt the V_1 - V_2 model [81]

$$V_1 \sum_{\langle ij \rangle} n_i n_j + V_2 \sum_{\langle\langle ij \rangle\rangle} n_i n_j, \quad (4)$$

with V_1 (V_2) the (next) nearest neighbor Coulomb repulsion. In the following, the next nearest neighbor hopping $t' = -0.05$ is also included to account for the FS revealed by angle-resolved photoemission spectroscopy (ARPES) [86–89]. The J -term in Eq. 3 is also kept. In the mean field calculations, we decouple the J -term in the pairing channel, and decouple the $V_{1,2}$ -terms in the charge bond channel. Exactly speaking, both the J and $V_{1,2}$ terms should be decoupled in all possible channels. Here, we take them as the effective interactions to drive PDW and CDW, respectively. In Fig. 4, we show two typical mean field solutions (more results can be found in Sec. III of the Supplementary Material). For the first case ($V_1 = 1$, $V_2 = 2$, $J = 1.2$, $n = 0.45$), the temperature dependence of the order parameters are shown in Fig. 4(a), indicating that the PDW can occur inside the CDW state with a lower T_c . Fig. 4(b) shows the ground state with coexisting (almost) real 3Q PDW and chiral CDW. Due to the chiral CDW background, the real 3Q PDW also acquires a weak chirality. This can be understood in the GL theory by considering the third-order coupling term

$$\gamma_3(\psi_1^* \psi_2 \phi_3 + \psi_2^* \psi_3 \phi_1 + \psi_3^* \psi_1 \phi_2 + \text{c.c.}), \quad (5)$$

where ψ_i/ϕ_i are PDW/CDW order parameters and γ_3 is the coupling strength. Clearly, the chiral CDW (complex ϕ_i) drives the chirality of PDW, regardless of the sign of γ_3 . Similarly, Figs. 4(f,g) show the results for the other case ($V_1 = 1.5$, $V_2 = 3$, $J = 1.6$, $n = 0.47$) with the chiral 3Q PDW occurring inside the chiral CDW state. Due to the chiral CDW background, the relative phases between each two PDW components deviate but only slightly from $2\pi/3$.

We see that the PDW can exist at a lower temperature inside the CDW phase due to the intertwining between these two types of orders. This makes it not only of theoretical interest but also a likely candidate for the superconductivity in AV_3Sb_5 . In particular, in a recent experiment [90], some signatures of the $2a_0 \times 2a_0$ PDW have been reported. In view of various experimental progresses, we present some supporting theoretical discussions. (1) We calculate the local Josephson currents $J_i(\theta)$ versus the Josephson phase difference θ (see Sec. I in Supplementary Material for technical details), as shown in Figs. 4(c,h) for the two mean field states, respectively. The critical current $J_{ic} = \max[J_i(\theta)]$, as measured in the scanning Josephson spectroscopy, shows a $2a_0 \times 2a_0$ period, which is consistent with the experiment. (2) The 3Q PDW states are fully gapped but the minimal gap is small, hence, behaving as gapless superconductors with “residual FSs” for realistic experiments with finite energy resolutions. Such a property can be used to distinguish

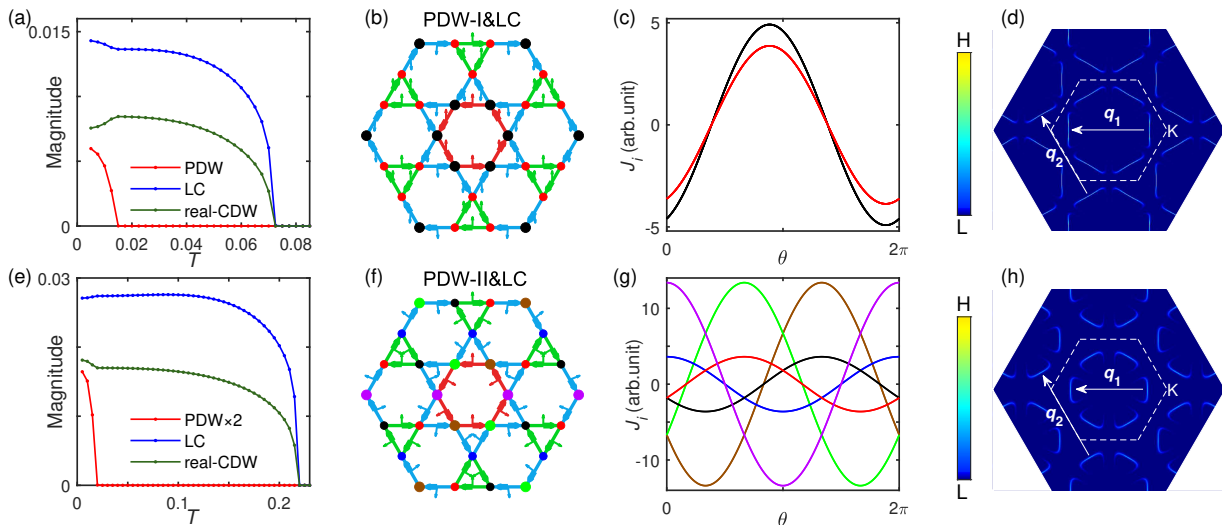


FIG. 4. (a-d) mean field results for $V_1 = 1$, $V_2 = 2$, $J = 1.2$, $n = 0.45$, including temperature-dependence of the order parameters in (a), PDW/CDW patterns in (b), local Josephson currents $J_i(\theta)$ in (c), and unfolded spectral function at zero energy in (d). The pattern convention in (b) is similar to Fig. 3, except the dot size now denotes n_i while the dot color indicates different line-shape of $J_i(\theta)$ in (c). (e-h) are similar plots to (a-d) but for $V_1 = 1.5$, $V_2 = 3$, $J = 1.6$, $n = 0.47$.

it from the usual SC. As examples, in Figs. 4(d,i), we plot the unfolded single-particle spectral function at zero energy with a realistic scattering rate $\eta = 0.005$, for the two mean field states, respectively. The “residual FSs” provide characteristic scattering vectors \mathbf{q}_1 and \mathbf{q}_2 (up to rotation symmetry), which should be visible in the quasi-particle interference (QPI) pattern (see Fig. S6 in Supplementary Material). We should note, however, that in order to make closer comparison to experiments, one has to take into account the multiple orbitals (or bands) into account, which are beyond our minimal model but deserve further elaborations. (3) The multi-Q (mQ) PDW provides a possibility to support fractional quantum flux $\Phi = \frac{1}{m} \sum_i W_i \Phi_0$ where $\Phi_0 = h/2e$ is the Abrikosov quantum flux and W_i is the winding number of ψ_i . This is a direct generalization of the two-component GL theory for the usual SC [91, 92], and provides an alternative to the charge-4e or -6e pairing to explain the experimentally-observed half or one-third quantum flux [93].

VI. SUMMARY

We have found robust $2a_0 \times 2a_0$ PDWs on the kagome lattice around the upper vH filling. The properties of

these PDWs are studied in GL and mean field theories. By further considering the CDW background, these PDWs are found to be consistent with some of the intriguing superconducting phenomena in AV_3Sb_5 . In particular, our work provide a minimal self-consistent model for the chiral $2a_0 \times 2a_0$ PDW ground state in the kagome lattice with broken time-reversal symmetry and exhibiting topological nontrivial features.

ACKNOWLEDGMENTS

This work is supported by National Key R&D Program of China (Grant No. 2022YFA1403201), National Natural Science Foundation of China (Grant No. 12374147, No. 12274205 and No. 92365203).

-
- [1] P. Fulde and R. A. Ferrell, *Phys. Rev.* **135**, A550 (1964).
 [2] A. I. Larkin and Y. N. Ovchinnikov, *Zh. Eksp. Teor. Fiz.* **47**, 1136 (1964).
 [3] M. W. Zwierlein, A. Schirotzek, C. H. Schunck, and W. Ketterle, *Science* **311**, 492 (2006).

- [4] G. B. Partridge, W. Li, R. I. Kamar, Y. an Liao, and R. G. Hulet, *Science* **311**, 503 (2006).
 [5] L. Radzihovsky and D. E. Sheehy, *Rep. Prog. Phys.* **73**, 076501 (2010).
 [6] P. A. Lee, *Phys. Rev. X* **4**, 031017 (2014).

- [7] E. Fradkin, S. A. Kivelson, and J. M. Tranquada, *Rev. Mod. Phys.* **87**, 457 (2015).
- [8] D. F. Agterberg, J. S. Davis, S. D. Edkins, E. Fradkin, D. J. Van Harlingen, S. A. Kivelson, P. A. Lee, L. Radzihovsky, J. M. Tranquada, and Y. Wang, *Annu. Rev. Condens. Matter Phys.* **11**, 231 (2020).
- [9] Q. Li, M. Hücker, G. D. Gu, A. M. Tsvelik, and J. M. Tranquada, *Phys. Rev. Lett.* **99**, 067001 (2007).
- [10] E. Berg, E. Fradkin, E.-A. Kim, S. A. Kivelson, V. Oganesyan, J. M. Tranquada, and S. C. Zhang, *Phys. Rev. Lett.* **99**, 127003 (2007).
- [11] D. F. Agterberg and H. Tsunetsugu, *Nat. Phys.* **4**, 639 (2008).
- [12] E. Berg, E. Fradkin, and S. A. Kivelson, *Nat. Phys.* **5**, 830 (2009).
- [13] M. H. Hamidian, S. D. Edkins, S. H. Joo, A. Kostin, H. Eisaki, S. Uchida, M. J. Lawler, E.-A. Kim, A. P. Mackenzie, K. Fujita, J. Lee, and J. C. S. Davis, *Nature* **532**, 343 (2016).
- [14] W. Ruan, X. Li, C. Hu, Z. Hao, H. Li, P. Cai, X. Zhou, D.-H. Lee, and Y. Wang, *Nat. Phys.* **14**, 1178 (2018).
- [15] S. D. Edkins, A. Kostin, K. Fujita, A. P. Mackenzie, H. Eisaki, S. Uchida, S. Sachdev, M. J. Lawler, E.-A. Kim, J. C. S. Davis, and M. H. Hamidian, *Science* **364**, 976 (2019).
- [16] Z. Shi, P. G. Baity, J. Terzic, T. Sasagawa, and D. Popović, *Nat. Commun.* **11**, 3323 (2020).
- [17] Z. Du, H. Li, S. H. Joo, E. P. Donoway, J. Lee, J. C. S. Davis, G. Gu, P. D. Johnson, and K. Fujita, *Nature* **580**, 65 (2020).
- [18] X. Li, C. Zou, Y. Ding, H. Yan, S. Ye, H. Li, Z. Hao, L. Zhao, X. Zhou, and Y. Wang, *Phys. Rev. X* **11**, 011007 (2021).
- [19] S. Wang, P. Choubey, Y. X. Chong, W. Chen, W. Ren, H. Eisaki, S. Uchida, P. J. Hirschfeld, and J. C. S. Davis, *Nat. Commun.* **12**, 6087 (2021).
- [20] C.-W. Cho, J. H. Yang, N. F. Q. Yuan, J. Shen, T. Wolf, and R. Lortz, *Phys. Rev. Lett.* **119**, 217002 (2017).
- [21] Y. Liu, T. Wei, G. He, Y. Zhang, Z. Wang, and J. Wang, *Nature* **618**, 934 (2023).
- [22] H. Zhao, R. Blackwell, M. Thinel, T. Handa, S. Ishida, X. Zhu, A. Iyo, H. Eisaki, A. N. Pasupathy, and K. Fujita, *Nature* **618**, 940 (2023).
- [23] Q. Gu, J. P. Carroll, S. Wang, S. Ran, C. Broyles, H. Siddiquee, N. P. Butch, S. R. Saha, J. Paglione, J. C. S. Davis, and X. Liu, *Nature* **618**, 921 (2023).
- [24] A. Aishwarya, J. May-Mann, A. Raghavan, L. Nie, M. Romanelli, S. Ran, S. R. Saha, J. Paglione, N. P. Butch, E. Fradkin, and V. Madhavan, *Nature* **618**, 928 (2023).
- [25] H. Chen, H. Yang, B. Hu, Z. Zhao, J. Yuan, Y. Xing, G. Qian, Z. Huang, G. Li, Y. Ye, S. Ma, S. Ni, H. Zhang, Q. Yin, C. Gong, Z. Tu, H. Lei, H. Tan, S. Zhou, C. Shen, X. Dong, B. Yan, Z. Wang, and H.-J. Gao, *Nature* **599**, 222 (2021).
- [26] C. C. Agosta, *Crystals* **8**, 285 (2018).
- [27] X. Liu, Y. X. Chong, R. Sharma, and J. C. S. Davis, *Science* **372**, 1447 (2021).
- [28] E. Berg, E. Fradkin, E.-A. Kim, S. A. Kivelson, V. Oganesyan, J. M. Tranquada, and S. C. Zhang, *Phys. Rev. Lett.* **99**, 127003 (2007).
- [29] E. Berg, E. Fradkin, S. A. Kivelson, and J. M. Tranquada, *New J. Phys.* **11**, 115004 (2009).
- [30] P. A. Lee, *Phys. Rev. X* **4**, 031017 (2014).
- [31] G. Y. Cho, R. Soto-Garrido, and E. Fradkin, *Phys. Rev. Lett.* **113**, 256405 (2014).
- [32] Y. Wang, D. F. Agterberg, and A. Chubukov, *Phys. Rev. Lett.* **114**, 197001 (2015).
- [33] Y. Wang, S. D. Edkins, M. H. Hamidian, J. C. S. Davis, E. Fradkin, and S. A. Kivelson, *Phys. Rev. B* **97**, 174510 (2018).
- [34] J.-T. Jin, K. Jiang, H. Yao, and Y. Zhou, *Phys. Rev. Lett.* **129**, 167001 (2022).
- [35] S. Zhou and Z. Wang, *Nat. Commun.* **13**, 7288 (2022).
- [36] S.-C. Zhang, *J. Phys. Chem. Solids* **59**, 1774 (1998).
- [37] A. Himeda, T. Kato, and M. Ogata, *Phys. Rev. Lett.* **88**, 117001 (2002).
- [38] M. Raczkowski, M. Capello, D. Poilblanc, R. Frésard, and A. M. Oleś, *Phys. Rev. B* **76**, 140505 (2007).
- [39] M. Capello, M. Raczkowski, and D. Poilblanc, *Phys. Rev. B* **77**, 224502 (2008).
- [40] K.-Y. Yang, W. Q. Chen, T. M. Rice, M. Sgrist, and F.-C. Zhang, *New J. Phys.* **11**, 055053 (2009).
- [41] F. Loder, A. P. Kampf, and T. Kopp, *Phys. Rev. B* **81**, 020511 (2010).
- [42] E. Berg, E. Fradkin, and S. A. Kivelson, *Phys. Rev. Lett.* **105**, 146403 (2010).
- [43] F. Loder, S. Graser, A. P. Kampf, and T. Kopp, *Phys. Rev. Lett.* **107**, 187001 (2011).
- [44] A. Jaefari and E. Fradkin, *Phys. Rev. B* **85**, 035104 (2012).
- [45] R. Soto-Garrido and E. Fradkin, *Phys. Rev. B* **89**, 165126 (2014).
- [46] R. Soto-Garrido, G. Y. Cho, and E. Fradkin, *Phys. Rev. B* **91**, 195102 (2015).
- [47] J. Wårdh and M. Granath, *Phys. Rev. B* **96**, 224503 (2017).
- [48] J. Wårdh, B. M. Andersen, and M. Granath, *Phys. Rev. B* **98**, 224501 (2018).
- [49] T. Sarkar, R. L. Greene, and S. Das Sarma, *Phys. Rev. B* **98**, 224503 (2018).
- [50] X. Y. Xu, K. T. Law, and P. A. Lee, *Phys. Rev. Lett.* **122**, 167001 (2019).
- [51] K. S. Huang, Z. Han, S. A. Kivelson, and H. Yao, *npj Quantum Mater.* **7**, 17 (2022).
- [52] Z. Han and S. A. Kivelson, *Phys. Rev. B* **105**, L100509 (2022).
- [53] Y.-M. Wu, P. A. Nosov, A. A. Patel, and S. Raghu, *Phys. Rev. Lett.* **130**, 026001 (2023).
- [54] Z. Wu, Y.-M. Wu, and F. Wu, *Phys. Rev. B* **107**, 045122 (2023).
- [55] Y.-M. Wu, Z. Wu, and H. Yao, *Phys. Rev. Lett.* **130**, 126001 (2023).
- [56] C. Setty, L. Fanfarillo, and P. J. Hirschfeld, *Nat. Commun.* **14**, 3181 (2023).
- [57] H.-C. Jiang, *Phys. Rev. B* **107**, 214504 (2023).
- [58] D. Shaffer, F. J. Burnell, and R. M. Fernandes, *Phys. Rev. B* **107**, 224516 (2023).
- [59] D. Shaffer and L. H. Santos, *Phys. Rev. B* **108**, 035135 (2023).
- [60] Y.-F. Jiang and H. Yao, “Pair density wave superconductivity: a microscopic model in two dimensions,” (2023), [arXiv:2308.08609](https://arxiv.org/abs/2308.08609) [cond-mat.supr-con].
- [61] Y.-M. Wu, R. Thomale, and S. Raghu, *Phys. Rev. B* **108**, L081117 (2023).
- [62] H.-K. Zhang, R.-Y. Sun, and Z.-Y. Weng, *Phys. Rev. B* **108**, 115136 (2023).

- [63] F. Chen and D. N. Sheng, *Phys. Rev. B* **108**, L201110 (2023).
- [64] C. Setty, J. Zhao, L. Fanfarillo, E. W. Huang, P. J. Hirschfeld, P. W. Phillips, and K. Yang, *Phys. Rev. B* **108**, 174506 (2023).
- [65] H.-C. Jiang and T. P. Devereaux, *Front. Electron. Mater.* **3**, 1323404 (2023).
- [66] F. Liu and Z. Han, *Phys. Rev. B* **109**, L121101 (2024).
- [67] A. Bose, S. Vadnais, and A. Paramakanti, "Altermagnetism and superconductivity in a multiorbital t-j model," (2024), [arXiv:2403.17050 \[cond-mat.str-el\]](https://arxiv.org/abs/2403.17050).
- [68] J. Wang, W. Sun, H.-X. Wang, Z. Han, S. A. Kivelson, and H. Yao, "Pair density waves in the strong-coupling two-dimensional holstein-hubbard model: a variational monte carlo study," (2024), [arXiv:2404.11950 \[cond-mat.str-el\]](https://arxiv.org/abs/2404.11950).
- [69] B. R. Ortiz, L. C. Gomes, J. R. Morey, M. Winiarski, M. Bordelon, J. S. Mangum, I. W. H. Oswald, J. A. Rodriguez-Rivera, J. R. Neilson, S. D. Wilson, E. Ertekin, T. M. McQueen, and E. S. Toberer, *Phys. Rev. Mater.* **3**, 094407 (2019).
- [70] B. R. Ortiz, S. M. L. Teicher, Y. Hu, J. L. Zuo, P. M. Sarte, E. C. Schueller, A. M. M. Abeykoon, M. J. Krogstad, S. Rosenkranz, R. Osborn, R. Seshadri, L. Balents, J. He, and S. D. Wilson, *Phys. Rev. Lett.* **125**, 247002 (2020).
- [71] N. Shumiya, M. S. Hossain, J.-X. Yin, Y.-X. Jiang, B. R. Ortiz, H. Liu, Y. Shi, Q. Yin, H. Lei, S. S. Zhang, G. Chang, Q. Zhang, T. A. Cochran, D. Multer, M. Litskevich, Z.-J. Cheng, X. P. Yang, Z. Guguchia, S. D. Wilson, and M. Z. Hasan, *Phys. Rev. B* **104**, 035131 (2021).
- [72] B. R. Ortiz, P. M. Sarte, E. M. Kenney, M. J. Graf, S. M. L. Teicher, R. Seshadri, and S. D. Wilson, *Phys. Rev. Mater.* **5**, 034801 (2021).
- [73] J.-X. Yin, B. Lian, and M. Z. Hasan, *Nature* **612**, 647 (2022).
- [74] T. Neupert, M. M. Denner, J.-X. Yin, R. Thomale, and M. Z. Hasan, *Nat. Phys.* **18**, 137 (2022).
- [75] K. Jiang, T. Wu, J.-X. Yin, Z. Wang, M. Z. Hasan, S. D. Wilson, X. Chen, and J. Hu, *Natl. Sci. Rev.* **10**, nwac199 (2023).
- [76] S. D. Wilson and B. R. Ortiz, *Nat. Rev. Mater.* , 1 (2024).
- [77] S.-L. Yu and J.-X. Li, *Phys. Rev. B* **85**, 144402 (2012).
- [78] M. L. Kiesel and R. Thomale, *Phys. Rev. B* **86**, 121105 (2012).
- [79] W.-S. Wang, Z.-Z. Li, Y.-Y. Xiang, and Q.-H. Wang, *Phys. Rev. B* **87**, 115135 (2013).
- [80] M. L. Kiesel, C. Platt, and R. Thomale, *Phys. Rev. Lett.* **110**, 126405 (2013).
- [81] J.-W. Dong, Z. Wang, and S. Zhou, *Phys. Rev. B* **107**, 045127 (2023).
- [82] Q.-G. Yang, M. Yao, D. Wang, and Q.-H. Wang, *Phys. Rev. B* **109**, 075130 (2024).
- [83] Y.-Q. Liu, Y.-B. Liu, W.-S. Wang, D. Wang, and Q.-H. Wang, *Phys. Rev. B* **109**, 075127 (2024).
- [84] A. Mine, Y. Zhong, J. Liu, T. Suzuki, S. Najafzadeh, T. Uchiyama, J.-X. Yin, X. Wu, X. Shi, Z. Wang, Y. Yao, and K. Okazaki, "Direct observation of anisotropic cooper pairing in kagome superconductor CsV3Sb5," (2024), [arXiv:2404.18472 \[cond-mat.supr-con\]](https://arxiv.org/abs/2404.18472).
- [85] U. Sivan and Y. Imry, *Phys. Rev. B* **33**, 551 (1986).
- [86] M. Kang, S. Fang, J.-K. Kim, B. R. Ortiz, S. H. Ryu, J. Kim, J. Yoo, G. Sangiovanni, D. Di Sante, B.-G. Park, C. Jozwiak, A. Bostwick, E. Rotenberg, E. Kaxiras, S. D. Wilson, J.-H. Park, and R. Comin, *Nat. Phys.* **18**, 301 (2022).
- [87] Y. Hu, X. Wu, B. R. Ortiz, S. Ju, X. Han, J. Ma, N. C. Plumb, M. Radovic, R. Thomale, S. D. Wilson, A. P. Schnyder, and M. Shi, *Nat. Commun.* **13**, 2220 (2022).
- [88] H. Li, D. Oh, M. Kang, H. Zhao, B. R. Ortiz, Y. Oey, S. Fang, Z. Ren, C. Jozwiak, A. Bostwick, E. Rotenberg, J. G. Checkelsky, Z. Wang, S. D. Wilson, R. Comin, and I. Zeljkovic, *Phys. Rev. X* **13**, 031030 (2023).
- [89] Y. Hu, X. Wu, A. P. Schnyder, and M. Shi, *npj Quantum Mater.* **8**, 67 (2023).
- [90] H. Deng *et al.*, Chiral superconductivity modulations with residual Fermi arcs, in preparation (2024).
- [91] M. Sigrist, T. M. Rice, and K. Ueda, *Phys. Rev. Lett.* **63**, 1727 (1989).
- [92] E. Babaev, *Phys. Rev. Lett.* **89**, 067001 (2002).
- [93] J. Ge, P. Wang, Y. Xing, Q. Yin, A. Wang, J. Shen, H. Lei, Z. Wang, and J. Wang, *Phys. Rev. X* **14**, 021025 (2024).